Chinese Chemical Letters 33 (2022) 4084–4088

Contents lists available at ScienceDirect

Chinese Chemical Letters

journal homepage: www.elsevier.com/locate/cclet

Sugar-dependent targeting and immune adjuvant effects of hyperbranched glycosylated polypeptide nanoparticles for ovalbumin delivery

Yingying Song, Chang-Ming Dong*

School of Chemistry and Chemical Engineering, Shanghai Key Laboratory of Electrical Insulation and Thermal Aging, Shanghai Jiao Tong University, Shanghai 200240, China

ARTICLE INFO

Article history:
Received 24 August 2021
Revised 14 January 2022
Accepted 17 January 2022
Available online 23 January 2022

Keywords:
Polypeptide nanoparticles
Sugar targeting
Immune adjuvant
Ovalbumin delivery system

ABSTRACT

Sugar-dependent targeting and immune adjuvant effects of hyperbranched glycosylated polypeptide nanoparticles were disclosed for ovalbumin (OVA) delivery system. The mannose-coated polypeptide nanoparticles can induce strongest targeting and immune adjuvant effects to macrophages than those glucose/lactose-coated ones, which effectively transported OVA into cells and facilitated OVA subcellular escape from endolysosomes into cytoplasm with the assistance of UV irradiation or intracellular acidic pH.

In the past decades, the biotherapeutics delivery systems including proteins/peptides, antigens, and antibodies have attracted increasing attention in immunotherapies of cancers and infectious diseases [1–3]. Besides intrinsic poor stability and short circulation half-lives, the major barriers such as poor membrane-impermeability, inefficient cellular trafficking and subcellular transport (*e.g.*, endolysosomes escape) are greatly limiting cytosolic protein delivery and therapeutic efficacy [4–6]. So it is imperative to develop high potent, specific/targeting, and safe protein delivery systems for various disease immunotherapies.

Owing to multiple tunable architectures and hierarchical self-assembly attributes, biodegradable and biocompatible polypeptides have intense appealing for constructing intelligent protein delivery systems, in which the built-in stimuli can be utilized to enhance cellular uptake and subcellular transportation of proteins [7–12]. Reminiscently, the glycocalyxes of branched glycoproteins and proteoglycans existing on cell surface and/or in extracellular matrice play unique adhesion, recognition, communication, inflammation, and immune response, implying that synthetic biomimetic glycosylated polypeptide (glycopolypeptide) would be a promising class of immune modulatory/stimulatory materials (*i.e.*, immune adjuvants) for protein delivery and immunotherapy [13–16]. Recently, Bertozzi *et al.* discovered that the bead-immobilized linear glycopolypeptide could activate antigen-presenting cells *via* dectin-1 and dectin-2 lectin receptors [17]. Various sugar-coated nanoparticles have also been studied as targeted OVA delivery systems to enchance OVA cellular uptake and boost immune response [18–22]. Interestingly, Chen *et al.* reported a glycopolymer engineering strategy to modify tumor and/or dendritic cells to trigger immune response [23]. Thus we reason that the cellular targeting and immune adjuvant effects of the glycopolypeptide nanoparticles on immune cells (*e.g.*, macrophage and dendritic cells) underpins an important rationale for designing highly potent immune adjuvants and related protein delivery systems.

To disclose the sugar-dependent targeting and immune adjuvant effects of the glycopolypeptide nanoparticles, herein we synthesized a small library of hyperbranched polypeptides with different photosensitive 2-nitrophenylethoxy (NPE), sugar and/or imidazole groups (Scheme S1 and Table S1 in Supporting information), which self-assembled into different sugar-coated micellar aggregates in phosphate buffer solution (PBS). Specifically, the UV-responsive hyperbranched poly(*N*ε-(1-(2-nitrophenyl)ethoxycarbonyl)-L-lysine) (HPNL) was directly photopolymerized from *N*ε-(1-(2-nitrophenyl)ethoxycarbonyl)-L-lysine-*N*-carboxyanhydride (NPE-Lys-NCA) without any addition of initiators/catalysts [24], which was further functionalized to afford the glucose-, lactose-, and/or mannose-decorated polypeptides (*i.e.*, HPG, HPL, HPM), and the pH-sensitive immidazolated one (*i.e.*, HPI), as characterized by ^{1}H NMR, GPC and the well-known ninhydrin test (Figs. S2-S4 and Table S1 in Supporting information) [25].

* Corresponding author.
E-mail address: cmdong@sjtu.edu.cn (C.-M. Dong).

https://doi.org/10.1016/j.cclet.2022.01.051
1001-8417/

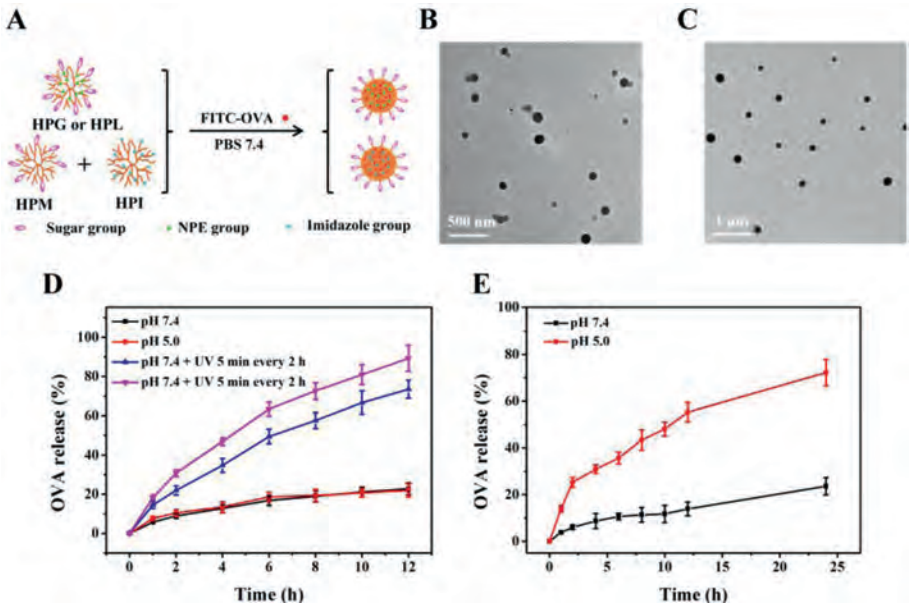

Fig. 1. Scheme for the preparation of sugar-coated and UV or pH sensitive nanoparticles (A); TEM photographs of (B) OVA-loaded HPL and (C) HPM/I nanoparticles; (D) UV-triggered OVA release from OVA-loaded HPL nanoparticles; (E) pH-triggered OVA release from OVA-loaded HPM/I nanoparticles.

Both HPG and HPL contained about 41% hydrophobic NPE groups and hydrophilic sugar residues, which self-assembled into the glucose- or lactose-coated and UV-sensitive spherical micellar aggregates and OVA-loaded ones in PBS, as characterized by DLS and TEM (Figs. 1A-C, Fig. S5 and Table S2 in Supporting information). These micellar aggregates presented similar UV-sensitive assembly and size increment behavior as intra/intermolecular hydrogen-bonding interactions drove the resulting glycosylated poly(L-lysine) (PLL) assemble into larger aggregates despite gradual photocleavage of NPE groups weakening hydrophobic and π-π interactions (Figs. S6 and S7 in Supporting information) [18,26]. Does the external UV stimulus triggered OVA release from those micellar aggregates in PBS? When UV-irradiation was turned on for 5 min and then off for 2 h, the released amount of FITC–OVA was greatly accelerated and increased up to about 73% within 12 h at pH 7.4 compared to the control with about 23% release at pH 7.4 or pH 5.0 (Fig. 1D), demonstrating the pulsatile UV-irradiation triggered a quick FITC–OVA release. With input of dual sequential triggers (*i.e.*, UV irradiation + pH 5.0), the FITC–OVA release further increased to about 89% within 12 h with the assistance of fast protonation of hyperbranched PLL wedges at an intracellular acidic pH. Meanwhile, the co-assembled HPM/I nanoparticles (HPM/HPI = 1/1, w/w) presented a pH-sensitive OVA release behavior due to fast protonation of imidazole groups at acidic pH 5.0, and the OVA release promptly increased from about 24% to 72% within 24 h when pH changed from 7.4 to 5.0 (Fig. 1E). The above external UV and intracellular acidic pH triggers would enable the sugar-coated micellar aggregates subcellular OVA trafficking, as in detail studied in the following.

As a simple and effective method, the lectin binding affinity with multiple sugar-coated nanoparticles can be used to assess the sugar-mediated cellular targeting effect because the immune cells (*e.g.*, macrophages and dendritic cells) overexpress lectin receptors such as macrophage galactose lectin (MGL) and mannose receptor (MR) [21,27]. So we tested specific binding activities of HPL, HPG, and HPM and HPM/I nanoparticles with the corresponding Con A and RCA_{120} lectins by means of on-line DLS and UV–vis spectroscopy. The mixed HPL/RCA_{120} aggregates dynamically increased from 60 nm to 450 nm and leveled off within 10 min (Fig. 2A), during which the solution turbidity increased accordingly (Fig. 2B). These results imply that the lactose-coated HPL nanoparticles dynamically bound with RCA_{120} and formed kinetically stable bigger aggregates. Similarly, the glucose-coated HPG nanoparticles also showed specific binding with Con A. However, when same concentration Con A was incubated with the mannose-coated HPM and HPM/I nanoparticles, the biggest aggregates dynamically formed in solution with turbidity increase by 6.9-fold and 6.0-fold than the glucose-coated ones (Table S3 in Supporting information). These findings implies that the mannose-coated HPM and HPM/I nanoparticles produced the strongest binding affinity with Con A compared to the glucose-/lactose-coated counterparts. That is to say, the mannose-coated nanoparticles would present more specific targeting effect to macrophages than the glucose-/lactose-coated ones, as further evidenced in the following cellular study.

Efficient cellular uptake of antigens is the first key step for the identification of antigens by immune cells (macrophages and dendritic cells), during which process macrophages prefer to specifically endocytose the galactose/lactose and mannose-coated nanoparticles *via* MGL and MR receptor-mediated endocytosis, respectively [21,27]. The intracellular uptake of OVA-loaded nanoparticles was monitored by time-dependent flow cytometry and fluorescent microscopy (Fig. 2C and Fig. S8 in Supporting information). At a dose of 10 μg/mL FITC–OVA equiv. and a fixed incubation time of 4 h, the fluorescence intensity clearly increased when the cells incubated with FITC–OVA loaded HPL or HPG nanoparticles compared to free FITC–OVA. Based on the mean fluorescence intensity (MFI) in Table S4 (Supporting information), it can be calculated that the antigen uptake increased 3.6 times for FITC–OVA loaded HPL nanoparticles and 2.5 times for FITC–OVA loaded HPG nanoparticles, respectively. The zeta potential of FITC–OVA loaded HPL nanoparticles was similar to that of HPG ones (38 mV *vs.* 31 mV), so the higher antigen uptake of the former resulted from specific binding of lactose-coated HPL nanoparticles with lectin receptors on macrophages. Remarkably, the antigen uptake increased 7.5 times for FITC–OVA loaded HPM nanoparticles and 4.4 times for FITC–OVA loaded HPM/I nanoparticles compared to free FITC–OVA. Taken together, the above results indicate that those different sugar-coated nanoparticles present sugar-dependent target-

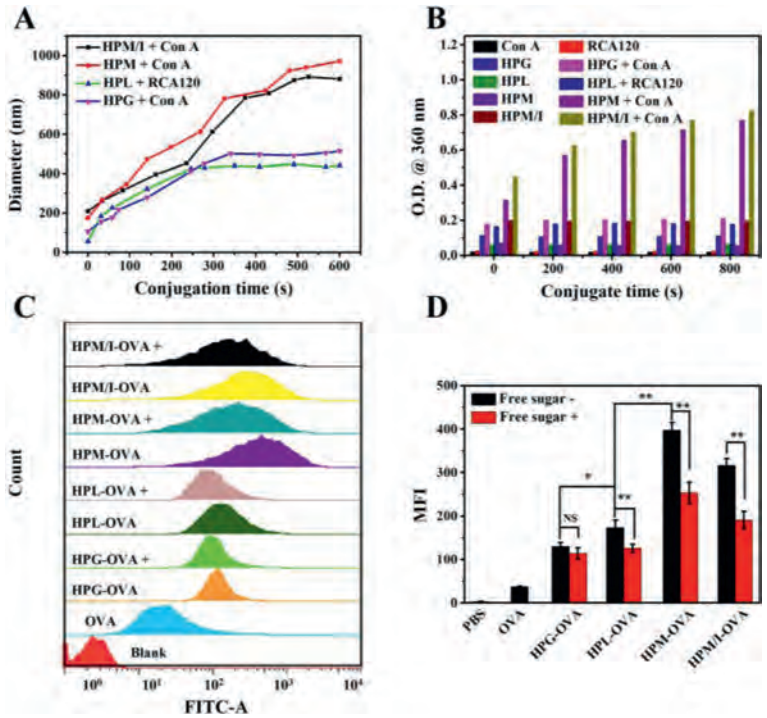

Fig. 2. (A) The changes of aggregates size and (B) optical density of HPL (40 μg/ mL) and HPM/I (40 μg/mL) after addition of RCA120 (0.5 mg/mL) or Con A (0.5 mg/mL); (C) Flow cytometry histogram profiles and (D) the MFI values of RAW264.7 cells incubated with free FITC–OVA, FITC–OVA loaded nanoparticles, and free sugar plus nanoparticles, "+" represents free sugar plus the corresponding sugar-coated nanoparticles.

ing effect to macrophages, and they are in the order of HPM > HPM/I > HPL > HPG nanoparticles.

To further prove the specific sugar-targeting effect, either galactose or mannose was selected to incubate with RAW264.7 cells for 1 h at 37 °C before addition of the HPL or HPG nanoparticles. As shown in Fig. 2D and Table S4 (Supporting information), the antigen uptake of the lactose-coated HPL nanoparticles was obviously inhibited with 27.7% decrease by the galactose addition. As for the mannose-coated HPM or HPM/HPI nanoparticles, the mannose addition decreased the uptake efficiency by 36.2% and 36.9%, respectively. However, free mannose had little impact on the antigen uptake of the glucose-coated HPG nanoparticles when incubated with RAW264.7 (MFI variation with $P > 0.05$). These findings demonstrated that the mannose-coated HPM or HPM/HPI nanoparticles and the lactose-coated HPL nanoparticles possessed specific sugar-targeting to RAW264.7 while the former was stronger than the latter, yet the glucose-coated HPG nanoparticles had no specific targeting ability.

Effective antigen escape from endolysosomes into cytoplasm is another key step for the antigen presentation and sequential immune response [2,12]. Endolysosomes and cell nuclei were stained by LysoTracker Red and Hoechst (blue), respectively, and subcellular antigen localization was assessed by CLSM. As shown in Fig. 3A, most internalized FITC–OVA loaded HPL nanoparticles colocalized in endolysosomes to become yellow after incubated with RAW264.7 cells for 4 h. However, upon UV-irradiation (5 min, 365 nm, 10 mW/cm^2), the green fluorescence intensified while yellow one weakened in cytoplasm. Moreover, the colocalization value between the green fluorescence and the red one in RAW264.7 cells obviously decreased from 68.0% to 41.7% upon UV irradiation (Fig. 3B and Table S5 in Supporting information). The UV irradiation triggered photosensitive NPE groups fall off and thus accelerated OVA release inside the cells while the proton sponge effect that was induced by fast protonation of hyperbranched PLL wedges made endolysosomes membrane rupture and sequential OVA escape into cytoplasm [12]. These results demonstrate that the UV irradiation not only triggered OVA release inside those macrophages but also facilitated endolysosomal OVA escape into cytoplasm (Fig. 4A). Furthermore, compared to external UV trigger, an effective subcellular transport of OVA can be implemented by intracellular acidic pH in a practicable manner. Comparing the FITC–OVA loaded HPM nanoparticles with the FITC–OVA loaded HPM/I nanoparticles, the colocalization value decreased from 71.6% to 42.9% due to the HPM/I nanoparticles having mixed imidazole and mannose corona. This result evidences that the endogenous acidic pH of endolysosomes was effective to accelerate OVA escape into cytoplasm as multivalent imidazole groups in hyperbranched PLL wedges boosted stronger proton sponge effect than their unmodified amino groups [19].

After endocytosis of extracellular antigens, nanoparticles, and/or antigen-laden nanoparticles, the macrophages would be activated and polarized into different phenotypes of M1 and M2, in which M1 phenotype mainly initiated adaptive immunity and secreted an important cytokine of tumor necrosis factor-α (TNF-α) while M2 intended to inhibit immunity [28]. The expression levels of M1-related CD86 and M2-related CD206 were estimated by flow cytometry (Fig. 4B and Table S6 in Supporting information) while the secreted TNF-α was assessed by ELISA (Fig. 4C and Table S7 in Supporting information). Both the expression level of CD86 and the TNF-α amount respectively increased with an order of HPM > HPM/I > HPL > HPG when treated with blank sugar-coated nanoparticles; HPM showed the highest increase of about 3.6-fold CD86 and 4.3-fold TNF-α, indicating that the mannose-coated polypeptide nanoparticles had the strongest immune adjuvant activity, which was consistent with the above sugar-dependent targeting activity. As a note, the sugar-coated polypeptide nanoparticles and the UV irradiation (5 min, 365 nm, 10 mW/cm^2) had no obvious cellular toxicity for the macrophages, respectively (Fig. S9 in Supporting information). In addition, the OVA-loaded HPL nanoparticles showed similar expression of CD86 and TNF-α (498.1

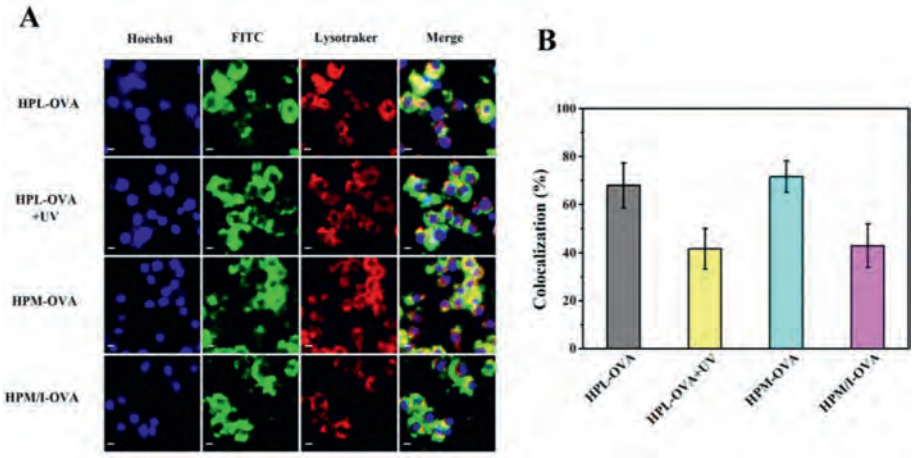

Fig. 3. (A) CLSM photographs and (B) the related colocalization values of those RAW264.7 cells incubated with different OVA-loaded polypeptide nanoparticles with/without UV irradiation ($n = 10$).

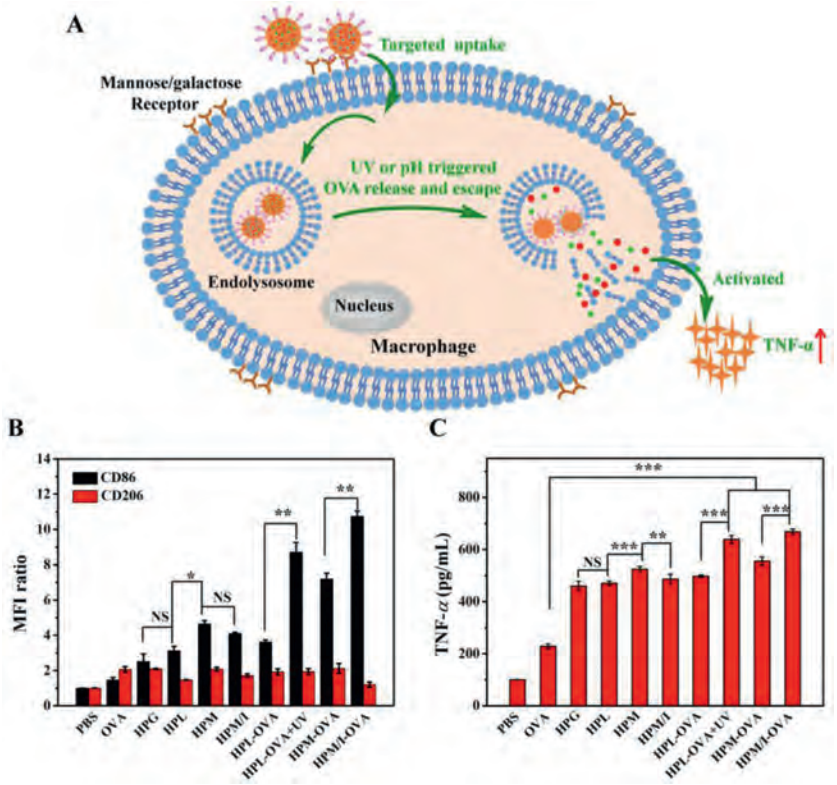

Fig. 4. (A) Illustration of those sugar-coated polypeptide nanoparticles mediating targeting uptake, UV or intracellular acidic pH triggered OVA release and subcellular escape, and the immune response; the expression levels of CD86 and CD206 (B) and the secreted TNF-α levels (C) of RAW264.7 when incubated with blank sugar-coated polypeptide nanoparticles and free FITC–OVA (10 μg/mL) or FITC–OVA loaded ones ($n = 3$, NS: none significance, $^{*}P < 0.05$, $^{**}P < 0.01$, $^{***}P < 0.001$).

pg/mL) to their blank ones, which was attributed to slow intracellular OVA release and poor endolysosomes escape without external or internal triggers. In contrast, upon UV irradiation, those OVA-loaded HPL nanoparticles significantly upregulated CD86 by 1.4-fold and induced a higher TNF-α of 639.0 pg/mL with 28.3% increment; and the ratio of M1/M2 dramatically increased from about 1.9 to 4.5, suggesting the macrophages were mainly polarized into M1. These results indicate that the UV irradiation indeed accelerated intracellular OVA release and facilitated subcellular endolysosomes trafficking, as confirmed by the above flow cytometry and CLSM analyses. Remarkably, the OVA-loaded HPM/I nanoparticles activated the highest CD86 expression and the ratio of M1/M2 increased from 2.4 to 8.9, thus inducing the highest TNF-α of 668.4 pg/mL by 37.4% increase than 486.5 pg/mL of the blank HPM/I nanoparticles and by 20.2% increase than 556.1 pg/mL of OVA-loaded HPM nanoparticles. This was because the acidic pH of endolysosomes could accelerate OVA release and trafficking into cytoplasm by the proton sponge effect of the imidazole groups on the surface of those HPM/I nanoparticles. Collectively, we can conclude that (1) all the mannose, lactose and glucose-coated polypeptide nanoparticles played key roles of immune adjuvants for activating the macrophages, in which the mannose-coated ones that had best targeting to macrophages presented best immune adjuvant effect, (2) either external UV irradiation or endogenous acidic pH could

trigger intracellular OVA release and simultaneously facilitate subcellular endolysosomes OVA escape into cytoplasm, mainly polarizing macrophages into M1, and (3) the combination of mannose and imidazole modifications would be a practicable strategy to endow the polypeptide nanoparticles targeting and immune adjuvant effects.

In summary, we synthesized a small library of hyperbranched polypeptides with different photosensitive NPE, sugar and/or imidazole groups, which self-assembled into different stimuli-sensitive and sugar-coated micellar aggregates. Those sugar-coated polypeptide nanoparticles presented sugar-dependent targeting and immune adjuvant effects to RAW264.7 cells, in which the mannose-coated ones that had best specific targeting presented best immune adjuvant effect than the lactose- or glucose-coated counterparts. Constructing the polypeptide nanoparticles with mixed mannose and imidazole corona is a practicable strategy for targeted OVA delivery to enhance immune response, opening up a new avenue for highly potent protein/antigen delivery and immunotherapy.

Declaration of competing interests

The authors declare that they have no known competing financial interests or personal relationships that could have appeared to influence the work reported in this paper.

Acknowledgment

The authors are grateful for the financial support of the National Natural Science Foundation of China (Nos. 22075176 and 21774074).

Supplementary materials

Supplementary material associated with this article can be found, in the online version, at doi:10.1016/j.cclet.2022.01.051.

References

[1] C.N. Fries, E.J. Curvino, J.L. Chen, et al., Nat. Nanotechnol. 16 (2021) 1–14.
[2] C.W. Shields IV, L.L.W. Wang, M.A. Evans, et al., Adv. Mater. 32 (2020) 1901633.
[3] K.T. Magar, G.F. Boafo, X. Li, et al., Chin. Chem. Lett. 33 (2022) 587–596.
[4] Y. Hu, L. Lin, Z. Guo, et al., Chin. Chem. Lett. 32 (2021) 1770–1774.
[5] Y.W. Lee, D.C. Luther, R. Goswami, et al., J. Am. Chem. Soc. 142 (2020) 4349–4355.
[6] L. Ren, J. Lv, H. Wang, et al., Angew. Chem. Int. Ed. 59 (2020) 4711–4719.
[7] A.R. Mazo, S. Allison-Logan, F. Karimi, et al., Chem. Soc. Rev. 49 (2020) 4737–4834.
[8] Z. Song, Z. Tan, J. Cheng, Macromolecules 52 (2019) 8521–8539.
[9] E. Liaroua, S. Varlas, D. Skoulas, et al., Prog. Polym. Sci. 83 (2018) 28–78.
[10] X. Liu, W. Gao, Angew. Chem. Int. Ed. 60 (2021) 11024–11035.
[11] Y. Miura, J. Mater. Chem. B 8 (2020) 2010–2019.
[12] L. Li, Z. Yang, X. Chen, Acc. Chem. Res. 53 (2020) 2044–2054.
[13] Z.S. Clauss, J.R. Kramer, Adv. Drug Deliver. Rev. 169 (2021) 152–167.
[14] L. Zeng, Z. Liao, W. Li, et al., Chin. Chem. Lett. 31 (2020) 1162–1164.
[15] B. Mondal, B. Pandey, N. Parekh, et al., Biomater. Sci. 8 (2020) 6322–6336.
[16] Z. Wang, Q. Chen, H. Zhu, et al., Chin. Chem. Lett. 32 (2021) 1888–1892.
[17] M.N. Zhou, C.S. Delaveris, J.R. Kramer, et al., Angew. Chem. Int. Ed. 57 (2018) 3137–3142.
[18] Y. Song, Y. Chen, P. Li, et al., Biomacromolecules 21 (2020) 5345–5357.
[19] D.S. Wilson, S. Hirosue, M.M. Raczy, et al., Nat. Mater. 18 (2019) 175–185.
[20] J. Conniot, A. Scomparin, C. Peres, et al., Nat. Nanotechnol. 14 (2019) 891–901.
[21] J.T. Wilson, Science 363 (2019) 584–585.
[22] W.J. Qi, Y.F. Zhang, J. Wang, et al., J. Am. Chem. Soc. 140 (2018) 8851–8857.
[23] L. Yu, R. Feng, L. Zhu, et al., Sci. Adv. 6 (2020) eabb6595.
[24] P. Li, Y.Y. Song, C.M. Dong, Polym. Chem. 9 (2018) 3974–3986.
[25] Z. Tian, M. Wang, A.Y. Zhang, et al., Polymer (Guildf) 49 (2008) 446–454.
[26] C.A. Machado, I.R. Smith, D.A. Savin, Macromolecules 52 (2019) 1899–1911.
[27] T. Mosaiab, D.C. Farr, M.J. Kiefel, et al., Adv. Drug Deliv. Rev. 151 (2019) 94–129.
[28] Z. Huang, J. Gan, Z. Long, et al., Biomaterials 90 (2016) 72–84.